adsorbed molecules is interpreting the images. How an adsorbed molecule influences tunneling efficiency, and particularly how different parts of a molecule may influence the tunneling efficiency differently, giving rise to the observed contrast in STM images, is poorly understood at best. Many mechanisms have been proposed to explain this contrast (*14*). One proposal is that the contrast is a result of interactions between the tunneling electrons and the molecular orbitals of the adsorbate. Several studies have shown a correlation between STM images and the single highest occupied molecular orbital (HOMO) or the lowest unoccupied molecular orbital (LUMO) of the adsorbed molecule (*15*). In several cases the HOMO and LUMO were sufficiently similar that it could not be determined if one, the other, or both were contributing to contrast in the STM image. Although adsorption may alter molecular orbital energies from their gas phase values, studies have suggested that this change is small (*16*).

To pursue this line of analysis, frontier molecular orbitals of MDW 74 were calculated by the Spartan (Wavefunction, Irvine, California) molecular modeling program. Calculations were performed at both semiempirical [modified neglect of differential overlap (MNDO)] and ab initio [Hartree–Fock/STO-3G (HF/STO-3G)] levels; except for absolute energies, the results were very similar. The orbitals calculated with MNDO (Fig. 3) showed that neither the single HOMO nor the single LUMO alone could explain the observed contrast because the HOMO and LUMO are each localized on one ring of the phenylbenzoate system, even though both rings appeared bright in the STM images. However, the observed contrast could be explained equally well by the group of four highest occupied orbitals (Fig. 3E), the group of four lowest unoccupied orbitals (Fig. 3C), or a combination of both (Fig. 3D).

The modeling work is summarized in Fig. 4, which shows a framework model of the 2D crystal computed by molecular mechanics with superimposed orbitals (LUMOs shown in Fig. 3C), along with the STM image itself. The one feature of the STM image that the model does not reproduce is the dissymmetry in the center of each column. Although it seems likely that this feature is associated with the epoxide group, their exact relationship is unclear. For a better test of the connection between molecular orbitals and STM images, high-resolution STM images of molecules possessing additional functional groups must be obtained.

REFERENCES AND NOTES

1. D. P. E. Smith, H. Hörber, Ch. Gerber, G. Binnig, *Science* **245**, 43 (1989).
2. For a recent review, see J. Frommer, *Angew. Chem. Int. Ed. Engl.* **31**, 1298 (1992).
3. Selected references: M. Shigeno *et al.*, *Jpn. J. Appl. Phys.* **29**, L119 (1990); D. P. E. Smith, *J. Vac. Sci. Technol. B* **9**, 1119 (1991); Y. Iwakabe *et al.*, *Jpn. J. Appl. Phys.* **30**, 2542 (1991).
4. J. K. Spong, L. J. LaComb Jr., M. M. Dovek, J. E. Frommer, J. S. Foster, *J. Phys. France* **50**, 2139 (1989); J. K. Spong *et al.*, *Nature* **338**, 137 (1989); J. S. Foster, J. E. Frommer, J. K. Spong, *SPIE* **1080**, 200 (1989); H. Shindo *et al.*, *Chem. Commun.* **1990**, 760 (1990); M. Hara, T. Umemoto, H. Takezoe, A. F. Garito, H. Sasabe, *Jpn. J. Appl. Phys.* **30**, L2052 (1991); S. L. Brandow *et al.*, *Liq. Cryst.* **13**, 163 (1993).
5. D. C. Parks, N. A. Clark, D. M. Walba, P. D. Beale, *Phys. Rev. Lett.* **70**, 607 (1993).
6. For the images in Fig. 1, the MDW 74 sample was >99% stereochemically pure at the epoxide stereocenters and about 80% stereochemically pure at the tertiary alkyl stereocenter (that is, the material was an 80:20 mixture of diastereomers differing at the tertiary alkyl stereocenter). Many other similar (though lower resolution) images were obtained with MDW 74 of >98% diastereomeric purity.
7. The current working hypothesis is that a very rare tip configuration produced the best STM images.
8. Only phenylbenzoates unsubstituted ortho to the ester moiety were chosen. The search found 57 fragments in 36 molecules. The minimum dihedral angle found was 42°; the average dihedral was 88°.
9. A. J. Groszek, *Proc. R. Soc. London Ser. A.* **314**, 473 (1970); U. Bien-Vogelsang and G. H. Findenegg, *Colloids Surf.* **21**, 469 (1986); G. H. Findenegg and M. Liphard, *Carbon* **25**, 119 (1987).
10. W. Mizutani, M. Shigeno, M. Ono, K. Kajimura, *Appl. Phys. Lett.* **56**, 1974 (1990).
11. D. P. E. Smith, W. M. Heckl, H. A. Klagges, *Surf. Sci.* **278**, 166 (1992); K. Matsushige *et al.*, *Jpn. J. Appl. Phys.* **32**, 1716 (1993).
12. Now Cerius[2].
13. Adiabatic dynamics, 300 K, 0.001-ps time step.
14. J.-Y. Yuan and Z. Shao, *Ultramicroscopy* **34**, 223 (1990); W. Mizutani, M. Shigeno, K. Kajimura, M. Ono, *ibid.* **42–44**, 236 (1992); M. M. D. Ramos, *J. Phys.: Condens. Matter* **5**, 2843 (1993); H. Ou-Yang, R. A. Marcus, B. Källebring, *J. Chem. Phys.* **100**, 7814 (1994).
15. P. H. Lippel, R. J. Wilson, M. D. Miller, Ch. Wöll, S. Chiang, *Phys. Rev. Lett.* **62**, 171 (1989); H. Nejoh, *Appl. Phys. Lett.* **57**, 2907 (1990); D. P. E. Smith, J. K. H. Hörber, G. Binnig, H. Nejoh, *Nature* **344**, 641 (1990); M. Shigeno, M. Ohmi, M. Suginoya, W. Mizutani, *Mol. Cryst. Liq. Cryst.* **199**, 141 (1991); S. Richter and Y. Manassen, *J. Phys. Chem.* **98**, 2941 (1994); C. Ludwig, B. Gompf, J. Petersen, R. Strohmaier, W. Eisenmenger *Z. Phys. B* **93**, 365 (1994).
16. A. J. Fisher, P. E. Blöchl, *Phys. Rev. Lett.* **70**, 3263 (1993); K.-H. Frank, R. Dudde, E. E. Koch, *Chem. Phys. Lett.* **132**, 83 (1986).

17. This work was supported in part by the Office of Naval Research and by the National Science Foundation (grants DMR-9202312 and DMR-9224168).

30 August 1994; accepted 6 December 1994

Optical Properties of the South Pole Ice at Depths Between 0.8 and 1 Kilometer

P. Askebjer, S. W. Barwick, L. Bergström, A. Bouchta, S. Carius, A. Coulthard, K. Engel, B. Erlandsson, A. Goobar,* L. Gray, A. Hallgren, F. Halzen, P. O. Hulth, J. Jacobsen, S. Johansson,† V. Kandhadai, I. Liubarsky, D. Lowder, T. Miller,‡ P. C. Mock, R. Morse, R. Porrata, P. B. Price, A. Richards, H. Rubinstein, E. Schneider, Q. Sun, S. Tilav, C. Walck, G. Yodh

The optical properties of the ice at the geographical South Pole have been investigated at depths between 0.8 and 1 kilometer. The absorption and scattering lengths of visible light (~515 nanometers) have been measured in situ with the use of the laser calibration setup of the Antarctic Muon and Neutrino Detector Array (AMANDA) neutrino detector. The ice is intrinsically extremely transparent. The measured absorption length is 59 ± 3 meters, comparable with the quality of the ultrapure water used in the Irvine-Michigan-Brookhaven and Kamiokande proton-decay and neutrino experiments and more than twice as long as the best value reported for laboratory ice. Because of a residual density of air bubbles at these depths, the trajectories of photons in the medium are randomized. If the bubbles are assumed to be smooth and spherical, the average distance between collisions at a depth of 1 kilometer is about 25 centimeters. The measured inverse scattering length on bubbles decreases linearly with increasing depth in the volume of ice investigated.

The AMANDA project was conceived to exploit polar ice as a transparent and sterile detection medium with a large volume for the detection of muons and neutrinos from astrophysical sources. Photomultiplier tubes (PMTs) deployed in the South Pole ice sense the Cherenkov light emitted by highly relativistic muons. Down-going muons originate from cosmic-ray showers, and nearly isotropic muons result from interactions between neutrinos and nucleons in the ice around and the bedrock below the detector. Polar ice, unlike ocean water which has also been proposed as a neutrino detector medium [for example, in the DUMAND (Deep Underwater Muon and Neutrino Detector) and NESTOR (neutrinos from supernovae and TeV sources, ocean range) experiments (*1*, *2*)], is free of bioluminescent organisms and natural radioactive isotopes such as ^{40}K. In addition, the ice forms a rigid support structure for the detector elements. At the low temperature of the medium, −55°C, the measured thermal noise rates average below 2 kHz per PMT.

One of the characteristic features of shallow polar ice is the abundance of air bubbles (3), which form as pockets of air become trapped between grains of snow (4). Microscopic examinations of ice-core samples from Greenland and Antarctica (5, 6) show that, at first, the size of air bubbles decreases with increasing depth (that is, pressure). When the hydrostatic pressure exceeds the formation pressure of air hydrates, a transition occurs during which the number of bubbles decreases. The hydrate crystals that form have a refractive index only 0.4% larger than that of pure ice (7), making scattering on these crystals negligible (8). At the Russian Antarctic station of Vostok, where the temperature of the ice is similar to that of the South Pole ice (the accumulation rate of snow and the altitude are, however, different), bubbles were not seen in ice cores below a depth of 1280 m, which sets an upper limit to the number density of air bubbles of 0.5 cm^{-3} (6). In the ice cores extracted from the Antarctic Byrd station, bubble-free ice was found below a depth of 1100 m (4).

Earlier measurements of the flux of Cherenkov photons from down-going cosmic-ray muons at a depth of 800 m with a prototype system consisting of four small PMTs (7.5-cm diameter) on a single string were tentatively interpreted to indicate that the South Pole ice was bubble-free at that depth (9). In this study, in which we used many more PMTs of larger size and a laser calibration system, we have now found clear indications of a residual density of air bubbles between 0.8 and 1 km, giving a very short scattering length of the Cherenkov light. The absorption of photons, however, is remarkably low. This makes the site, at deeper levels, essentially free from air bubbles and very promising for the AMANDA detector.

During the Antarctic summer of 1993–1994, four strings, each equipped with 20 PMTs (20-cm diameter), were installed at depths between 800 and 1000 m in the South Pole ice as shown in Fig. 1. Along with the main signal cable carrying the high voltage and the PMT signals were optical fibers that carry light from a laser calibration source at the surface to each optical module. Each optical fiber terminates in a diffusive nylon sphere placed about 30 cm from the PMT. By sending laser pulses to individual nylon spheres and measuring the photon travel-time distributions between modules (time resolution, ~5 ns), the optical properties of the medium can be derived. The intensities of the laser pulses coming out of the spheres are high enough that photons are detected by PMTs in neighboring strings. The calibration pulses have a wavelength of 515 ± 15 nm. The travel times of photons between the emitting nylon sphere and the receiving optical modules were many times longer than what would be expected from a straight path. Figure 2, A and B, shows two examples of such measurements. With no obstacles, the signals would have arrived after 91 ns in Fig. 2A and after 142 ns in Fig. 2B.

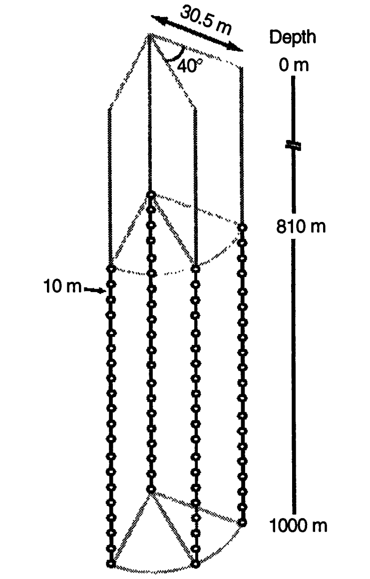

Fig. 1. The AMANDA detector. The four strings were deployed between December 1993 and January 1994. We drilled a hole in the ice 60 cm wide for each string by pumping water at 90°C at a rate of 40 gallons per minute. The time needed to drill a hole was less than 90 hours, typically 4 days. The holes are vertical within 1-mrad precision. There are 20 modules in each string, spaced 10 m apart. Each PMT is contained inside a pressure vessel. An optical fiber carries laser light from the ice surface to a diffusive nylon sphere suspended below each PMT.

A model for the distribution of the photon travel times can be constructed, if we assume that the time delays are caused by collisions with air bubbles. The scattering length on spherical bubbles—that is, the average distance that a photon travels between collisions with bubbles—is given by

$$\lambda_{bub} = \frac{1}{n_{bub}\langle \pi r^2 \rangle_{bub}} \qquad (1)$$

where n_{bub} is the number density of bubbles and $\langle \pi r^2 \rangle_{bub}$ is their average geometrical cross section. Dust particles, although present in glacier ice with a comparable number density, typically have radii that are 1/10 to 1/100 that of air bubbles—that is, the collision rate between photons and insoluble dust particles can be neglected in the presence of air bubbles (8).

If the light is detected at the PMT after a large number of scatterings, the situation can be described as a random-walk (diffusive) process. We need to incorporate only two modifications to the standard random-walk treatments given in the literature (10)—namely, absorption of light and the

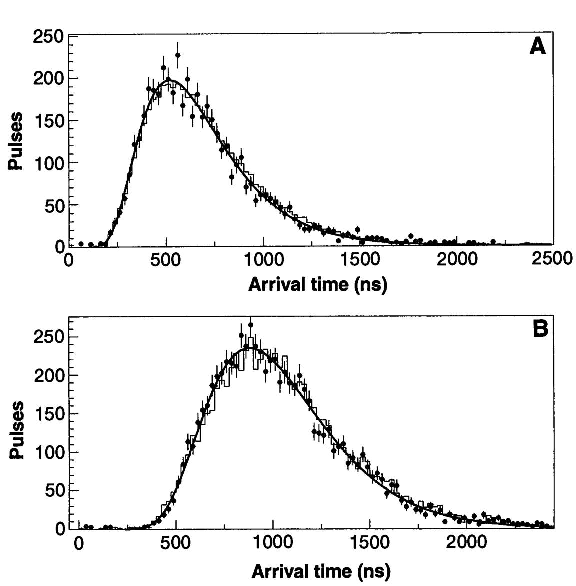

Fig. 2. Arrival-time distributions for two different source-detector separations. The data points (dots) are compared to the Monte Carlo simulation (histogram) and to the fits of Eq. 5 (solid line). The emitting and receiving PMTs are 21 m apart in (**A**) and 32 m apart in (**B**).

P. Askebjer, L. Bergström, A. Bouchta, B. Erlandsson, A. Goobar, P. O. Hulth, S. Johansson, Q. Sun, C. Walck, Stockholm University, Box 6730, S-11385 Stockholm, Sweden.
S. W. Barwick, P. C. Mock, R. Porrata, E. Schneider, G. Yodh, University of California, Irvine, CA 92717, USA.
S. Carius, A. Hallgren, H. Rubinstein, Uppsala University, Box 535, S-75121 Uppsala, Sweden.
A. Coulthard, K. Engel, L. Gray, F. Halzen, J. Jacobsen, V. Kandhadai, I. Liubarsky, R. Morse, S. Tilav, University of Wisconsin, Madison, WI 53706, USA.
D. Lowder, T. Miller, P. B. Price, A. Richards, University of California, Berkeley, CA 94720, USA.

*To whom correspondence should be addressed.
†Present address: Jönköping University, Box 1026, S-55111 Jönköping, Sweden.
‡Present address: Bartol Research Institute, Newark, DE 19716, USA.

All the authors are affiliated with the AMANDA collaboration.

nonisotropy of the scattering amplitude for photons incident on air bubbles.

Absorption can be taken into account by the factor $e^{\frac{-N\lambda_{bub}}{\lambda_a}}$ for each path of N steps (we assume $N \gg 1$; typically, N is on the order of 1000 in our problem), where λ_a is the absorption length. Nonisotropy of the scattering means that there is a correlation between successive vectors making up the random walk. If the bubbles are spherical, there is still an azimuthal symmetry, and one can show that (by introducing rotation matrices that rotate each successive vector to the polar axis)

$$\langle \mathbf{r}_1 \cdot \mathbf{r}_{1+k} \rangle = \lambda^2_{bub}(\delta_{0,k} + \tau^k) \qquad (2)$$

where $\tau = \langle \cos\theta \rangle$ is the average of the cosine of the scattering angle.

In the formula for random walk with absorption (*11*)

$$W_N(\mathbf{R}) = \frac{1}{(2\pi\langle \mathbf{R}^2\rangle_N/3)^{3/2}} e^{-\frac{3\mathbf{R}^2}{2\langle \mathbf{R}^2\rangle_N}} e^{\frac{-N\lambda_{bub}}{\lambda_a}} \qquad (3)$$

where $W_N(\mathbf{R})$ is the probability function for reaching $\mathbf{R}$ after N steps and

$$\langle \mathbf{R}^2\rangle_N = \langle (\sum_{j=1}^{N} \mathbf{r}_j)^2 \rangle$$
$$\propto 2N\lambda^2_{bub}[1 + \tau + \tau^2 + \tau^3 + \ldots + \mathcal{O}(1/N)]$$
$$= \frac{2N\lambda^2_{bub}}{1-\tau} \qquad (4)$$

With the identification $N\lambda_{bub} = c_i t$, where $c_i = c/n$ is the velocity of light in the ice, we obtain the formula corresponding to the Green's function for the radiative transport of a spherically symmetric light pulse emitted at a distance $d = 0$ at time $t = 0$

$$u(d,t) = \frac{1}{(4\pi Dt)^{3/2}} e^{\frac{-d^2}{4Dt}} e^{\frac{-c_i t}{\lambda_a}} \qquad (5)$$

where $u(d,t)$ is the density of photons (normalized to unity at $t = 0$) at a distance d from the source at time t. The diffusion constant D is given by

$$D = \frac{c_i \lambda_{eff}}{3} \qquad (6)$$

with the effective scattering length λ_{eff} related to λ_{bub} through the formula

$$\lambda_{eff} = \frac{\lambda_{bub}}{1-\tau} \qquad (7)$$

In the expression for D, only the refractive scattering part of the optical amplitude has to be taken into account. If diffraction is included, which would cause the effective cross section of the bubble to increase from σ to $(B + 1)\sigma$ (where B is an arbitrary constant) (*12*), then $\lambda_{bub} \rightarrow \lambda_{bub}/(1 + B)$, $\tau \rightarrow (B + \tau)/(B + 1)$, and D is easily seen to be invariant under these transformations.

The distributions of arrival times were also calculated in a Monte Carlo simulation. Because of the existence of widely separated length scales, $d \sim \lambda_a \gg \langle r_{bub} \rangle \gg \lambda_L$, where λ_L is the wavelength of the laser light, a fairly simple optical treatment is adequate for this analysis. In fact, the estimate of λ_a is obtained almost directly from the falloff of the arrival times of late photons and is fairly insensitive to the uncertainties in the determination of λ_{bub}.

The initial state in any single scattering can be regarded as being completely incoherent. We have thus used simple geometrical optics for the scattering process incorporating singly refracted light, externally reflected light, and totally reflected light with the relative strengths of the components given by the Fresnel coefficients. We took into account the change in the refractive index of the air in the bubbles, assuming hydrostatic pressure. For the ice, we used the value of the refractive index, $n = 1.31$, given in (*13*). With our approximations, we found for spherical, smooth bubbles [as observed in ice-core samples from the Antarctic Byrd station (*4*)] that τ in Eq. 7 takes a value of ~0.75 (corresponding to an average scattering angle of 41°).

In Fig. 2 we show a comparison of the experimental data, the results of our Monte Carlo simulations, and the analytical formula of Eq. 5. The best fit to the data gives a value for λ_{bub} of 0.19 m in both Figs. 2A and 2B, and a value for λ_a of 61 m in Fig. 2A and 60 m in Fig. 2B. The agreement between the Monte Carlo simulations (run with the above parameters), the data, and the analytical fit is quite remarkable. We thus conclude that the physics behind the PMT calibration data is well understood and that we have at our disposal a tool with which to measure properties of the ice such as λ_a and λ_{eff}. These quantities are uniquely determined by the temporal distribution of photons at each particular PMT, once the geometry of the detector array is fixed.

A global χ^2 minimization of the time data was performed where the relative vertical distances between the strings were left as free parameters, λ_a was assumed to be a constant, and $1/\lambda_{bub}$ was expressed as a linear function of depth. Although all the optical modules are equipped with an optical fiber and a nylon sphere, only 12 of them could be pulsed before the members of the AMANDA experiment had to leave the site in February 1994. For our analysis, we have selected time distributions where at least 1000 pulses were registered by the receiving PMT. The time measured is set by the arrival of the first photon. In order to reproduce the true time distribution given by the different photon paths in the medium, we selected distributions for which the probability that more than one photon would be detected at the receiving PMT for each trigger is less than 6%. A total of 36 time distributions like the ones shown in Fig. 2 was used in the global fit.

The optical properties of the medium are parameterized as described in Eq. 5. Only statistical uncertainties in the number of detected photons were considered. The relative vertical positions of the four strings were determined to a precision of ~0.2 m. For the absorption length and the inverse scattering length on air inclusions, the global fit yields $\lambda_a = 59 \pm 1$ m and

$$\frac{1}{\lambda_{bub}} = \frac{(28.6 \pm 1.1) - (0.025 \pm 0.001)z}{4(1-\tau)} \text{ m}^{-1} \qquad (8)$$

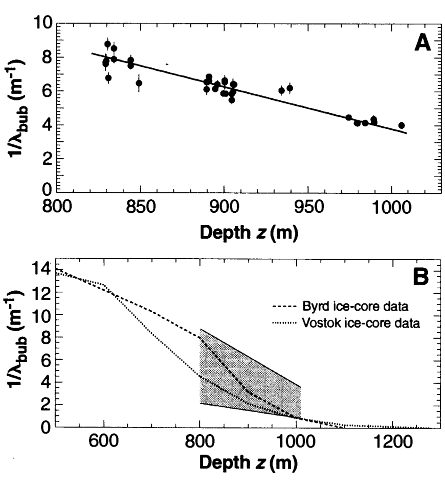

Fig. 3. Inverse scattering length $1/\lambda_{bub}$ as a function of depth z. The data points in (**A**) are AMANDA measurements shown together with the best fitted linear dependence of Eq. 8 for $\tau = 0.75$ (that is, spherical bubbles). The fitted line extrapolates to zero at ~1150 m. The shaded area in (**B**) shows the AMANDA results allowing for $\tau = 0 - 0.75$ ($\tau = 0$ corresponds to isotropic scattering). Also shown are the Byrd and Vostok ice-core measurements (*4*, *6*), where we have computed an equivalent value of λ_{bub} from their quoted bubble number density (N) and the square of the average bubble radius (ρ^2), $1/\lambda_{bub} = N\pi\rho^2$.

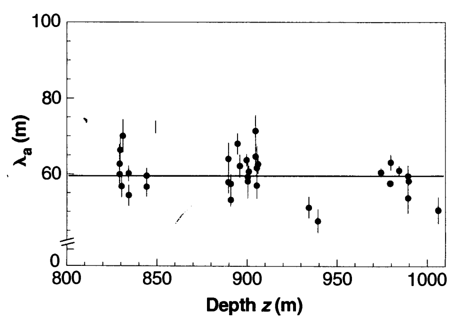

Fig. 4. Measured absorption length, λ_a, at depths between 0.8 and 1 km. The solid line shows the best fitted value.

where z is the vertical depth (in meters), defined to be zero at the surface and increasing downward. We used Monte Carlo simulations to estimate the systematic uncertainties in the global fit from the contamination of multiple-photon events, background events, and limited sample sizes. We find that the various effects tend to cancel each other. A conservative estimate of the total uncertainty in λ_a is

$$\lambda_a = 59 \pm 1(\mathrm{stat}) \pm 3(\mathrm{syst})\ \mathrm{m} \quad (9)$$

Figure 3A shows the observed linear dependence of $1/\lambda_{bub}$ on depth. This depth dependence is steeper than would be expected if the bubble number density were constant and only the bubble sizes decreased under the hydrostatic pressure ($1/\lambda_{bub} \propto z^{-2/3}$). The shaded area in Fig. 3B corresponds to the uncertainty in the bubble shapes—that is, in the average scattering angle. Also shown in Fig. 3B are results from the measurements on the Vostok and Byrd ice cores. Figure 4 shows the measured absorption lengths at different depths.

We measured the propagation parameters of visible light in the South Pole ice to an accuracy of ~5%, using the calibration setup of the AMANDA detector (these measurements were made without extracting ice samples). The small uncertainty in the measured value of λ_a was achievable only because of the long travel times of photons in the bubbly ice. Alternative explanations to the observed photon time distributions (such as that the time distributions are caused by fluorescence in the medium) are extremely unlikely. Our results are also incompatible with a localized bubble concentration as the cause of the observed time smearing. The examined ice volume, 0.8 to 1 km below the surface, has an extremely long absorption length, comparable with the quality of the ultrapure water used in the IMB and Kamiokande proton-decay and neutrino experiments (*14*, *15*) and more than twice as long as the best value reported for laboratory ice (*13*).

The results of this study suggest that the ice cap is indeed an ideal medium for a neutrino telescope. If the absorption length does not deteriorate with depth, the volume of a future muon and neutrino detector to be deployed at greater depth can be made significantly larger than previously anticipated because the PMTs can be spaced farther apart. A linear extrapolation of our data would indicate that bubbles vanish at ~1150 m at the South Pole. The data from Vostok and Byrd (Fig. 3B) show, however, that the rate of bubble disappearance becomes somewhat slower toward the end of the transition process (*16*).

REFERENCES AND NOTES

1. P. K. F. Grieder, talk given at "Trends in Astroparticle Physics," Stockholm, September 1994 [*Nucl. Phys. B* (suppl.), in press].
2. NESTOR Collaboration, in *Proceedings of the Workshop on High Energy Neutrino Astrophysics*, V. J. Stenger *et al.*, Eds. (World Scientific, Singapore, 1992).
3. H. Shoji and Ch. C. Langway Jr., *Nature* **298**, 548 (1982).
4. A. J. Gow and T. Williamson, *J. Geophys. Res.* **80**, 5101 (1975).
5. H. Shoji and Ch. C. Langway Jr., *J. Phys.* (*Paris*) (*Suppl. 3*) **48**, C1-551 (1987).
6. N. I. Barkov and V. Ya. Lipenkov, *Mater. Glyatsiolog. Issled.* **51**, 178 (1985).
7. T. Hondoh *et al.*, *J. Incl. Phen.* **8**, 17 (1990); T. Uchida, personal communication.
8. AMANDA Collaboration (P. Askebjer *et al.*), in preparation.
9. T. Miller *et al.*, in *Proceedings of 23rd International Cosmic Ray Conference*, D. A. Leahy *et al.*, Eds. (World Scientific, Singapore, 1993), vol. 4, p. 557.
10. S. Chandrasekhar, *Rev. Mod. Phys.* **15**, 1 (1943).
11. A. Ishimaru, *J. Opt. Soc. Am.* **68**, 8 (1978); M. S. Patterson *et al.*, *Appl. Opt.* **28**, 12 (1989).
12. H. C. van de Hulst, *Light Scattering by Small Particles* (Wiley, New York, 1957).
13. T. C. Grenfell and D. K. Perovich, *J. Geophys. Res.* **86**, 7447 (1981); S. G. Warren, *Appl. Opt.* **23**, 1206 (1984).
14. R. Becker-Szendy *et al.*, *Nuclear Instrum. Methods*, in press.
15. K. Inoue, thesis, Institute of Cosmic Ray Research, University of Tokyo (1993).
16. During the Antarctic summer of 1994–1995, we plan to collect new calibration data with the same system to establish the wavelength dependence of the optical properties of the South Pole ice (P. Askebjer *et al.*, in preparation).

17. We thank B. Koci and the entire Polar Ice Coring Office organization for support with the ice drilling. This work was supported by the National Science Foundation (USA), the K. A. Wallenberg Foundation (Sweden), the Swedish Natural Science Research Council, the G. Gustafsson Foundation (Sweden), Swedish Polar Research, the Graduate School of the University of Wisconsin, Madison (USA), and the University of California at Irvine (USA).

24 August 1994; accepted 13 December 1994

Viscous Dissipation in Three-Dimensional Convection with Temperature-Dependent Viscosity

S. Balachandar,* D. A. Yuen, D. M. Reuteler, G. S. Lauer

Numerical simulations of three-dimensional convection with temperature-dependent viscosity and viscous heating at realistic Rayleigh numbers for Earth's mantle reveal that, in the strongly time-dependent regime, very intense localized heating takes place along the top portion of descending cold sheets and also at locations where the ascending plume heads impinge at the surface. For a viscosity contrast of 100, these localized heat sources exceed the internal heating due to the radioactive decay of chondritic materials by more than an order of magnitude. The horizontally averaged viscous dissipation is concentrated in the top of the convecting layer and has a magnitude comparable with that of radioactive heating.

Viscous dissipation is an irreversible process accompanying fluid motion and has generally been studied in the high Mach number regimes. However, even at the low speeds of fluid motion in Earth's mantle, the contribution from viscous heating can be significant because of the great distances involved (*1*). This potentially important role played by viscous heating and its coupling to temperature-dependent viscosity on mantle dynamics has long been recognized (*2*–*5*). Recent two-dimensional (2D) time-dependent studies (*6*) have shown that viscous heating can trigger heating instabilities in the transition zone as a result of the interaction of a hot plume with the endothermic phase transition (*7*). In this report, we investigate the phenomenon of viscous heating coupled with the temperature-dependent viscosity in three dimensions at high Rayleigh numbers and discuss the nature of the intense shear heating that is produced both in hot rising plumes and along the descending cold sheets. Such localized heating helps explain the source of hot anomalies adjacent to subducting regions (*8*) and the thinning of the lithosphere above hot upwellings (*9*). This phenomenon of localized viscous heating does not occur in the ordinary Boussinesq convection, which can be studied in laboratory experiments (*10*), but instead must be studied numerically.

We used a spectral-transform technique (*11*) to solve the relevant conservation equations. The numerical model includes the effects of both viscous heating and adiabatic cooling but no internal heating. We considered an aspect ratio of 5 by 5 by 1, with unity being the depth of the layer. The dimensionless equations for the conservation of mass, momentum, and energy in terms of the nondimensional velocity **u**, temperature T, and dynamical

S. Balachandar, Department of Theoretical and Applied Mechanics, University of Illinois, Urbana, IL 61801, USA.
D. A. Yuen, D. M. Reuteler, G. S. Lauer, Minnesota Supercomputer Institute and Department of Geology and Geophysics, University of Minnesota, Minneapolis, MN 55415, USA.

*To whom correspondence should be addressed.